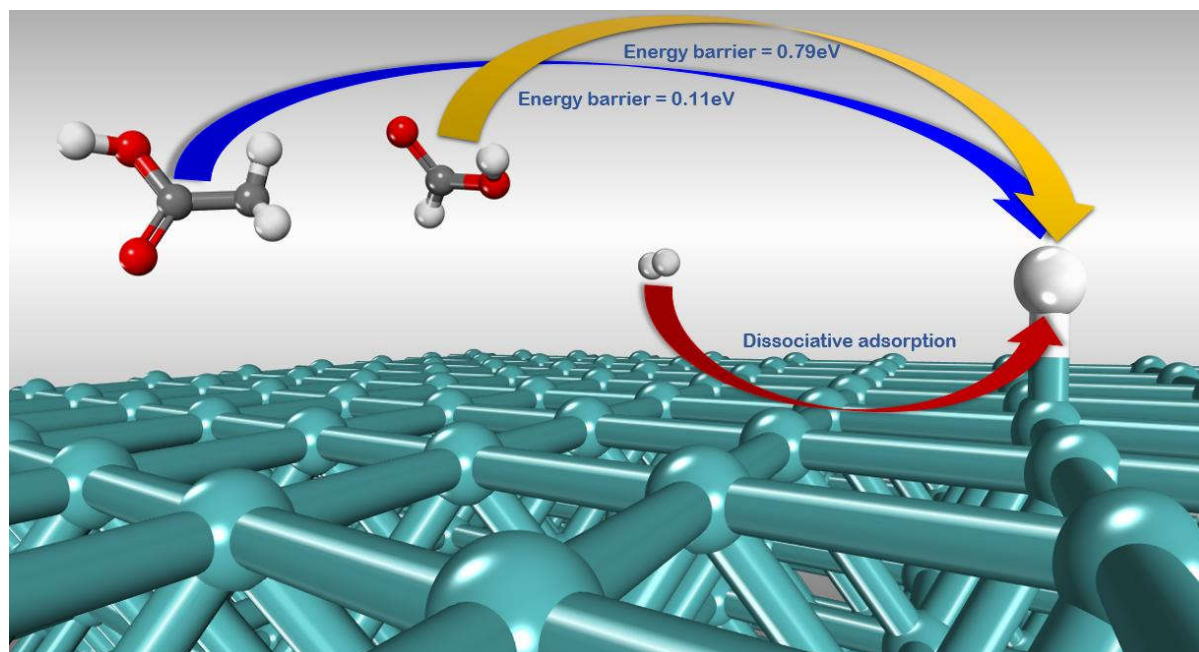


Graphical Abstract



Highlights

- Hydrogen donation in catalytic decomposition of bio-acids and H_2 was investigated.
- Ten transition metals were tested for bio-acid adsorption.
- Electron density difference was analysed to elucidate interface interaction.
- Mo showed good effects in facilitating the decomposition of bio-acids.
- AcOH had good potential as an alternative hydrogen donor compound over Mo (110).

1 **Hydrogen donation of bio-acids over transition metal facets:**
2 **A Density Functional Theory study**

3 Jiajun Zhang^{ac}, Xiaolei Zhang^{ac*}, Amin Osatiashtiani^b, Anthony Bridgwater^b

4 * Corresponding author: X.Z., E-mail address: xiaolei.zhang@strath.ac.uk

5 ^aDepartment of Chemical and Process Engineering, University of Strathclyde,
6 Glasgow, United Kingdom

7 ^b European Bioenergy Research Institute (EBRI), School of Engineering and Applied
8 Science, Aston University, Aston Triangle, Birmingham, B4 7ET, United Kingdom

9 ^c School of Mechanical and Aerospace Engineering, Queen's University Belfast,
10 Belfast, United Kingdom

11 **Abstract**

12 Bio-acids produced from biomass fast pyrolysis are regarded as alternative hydrogen
13 source for upgrading bio-oil into transport fuels. In this work, the hydrogen donation
14 performance of acetic acid (AcOH) and formic acid (FA) were evaluated over the
15 transition metal facet in comparison with H₂ gas, using Density Functional Theory (DFT)
16 modelling. It was revealed that Mo (110) led to stronger binding with the bio-acid
17 molecule than other base transition metals, and the consequent electrons migration
18 significantly facilitated the bio-acids decomposition. AcOH exhibited a greater potential
19 than FA as a hydrogen donor over Mo (110) because it released more H atoms with
20 low energy barriers. H₂ gas showed undoubtable merits of dissociative adsorption with
21 negligible energy barrier over Mo (110). However, the larger enthalpy changes from the
22 exothermic decomposition of bio-acids would probably more facilitate the activation and
23 migration of the individual H atoms for their donation compared to H₂ gas.

24 **Abbreviations:** Acetic Acid, AcOH; Formic Acid, FA; Aromatic Hydrocarbons, AHs;

25 Electronic density difference, EDD

26

27 **Key words:** Hydrogen donor compounds; Catalytic decomposition;

28 Hydrodeoxygenation; DFT modelling; Transition metals

29

30 **1. Introduction**

31 Nowadays biofuel is an attractive alternative fuel because it can lower our dependency
32 on conventional fossil fuels, achieve “zero” net carbon emissions, and tackle the
33 challenge of global warming [1]. Thermochemical conversion of waste biomass via
34 catalytic fast pyrolysis offers a promising route to biofuels. However, the direct use of
35 bio-oil is hindered by its undesirable physicochemical properties such as low calorific
36 value due to its high oxygen content and water content, high viscosity and low stability
37 owing to its high acid content. This explains why upgrading is being so intensively
38 studied. Hydrodeoxygenation (HDO) is considered an effective method for upgrading
39 bio-oil to more valuable and useful liquid products [2]. Conventionally, molecular H₂ gas
40 is used in industrial HDO processes, because of its dissociation on the surface of the
41 catalysts, thus providing high reactivity. However, there are some drawbacks
42 associated with the application of molecular H₂ gas such as the high process costs due
43 to high-pressure reactors, concerns over process safety regarding H₂ storage and
44 utilisation, the requirement to recover and recycle hydrogen. Additionally, using pure H₂
45 during HDO may lead to the saturation of aromatic rings, producing undesired
46 cycloalkanes instead of aromatic hydrocarbons. Therefore, alternative sustainable
47 hydrogen sources are urgently sought-after to address the challenges of developing an
48 efficient and cost effective HDO process.

49 Much effort has been devoted to finding the alternative hydrogen sources, and it has
50 been reported that hydrogen can be produced in-situ via various reactions [2,3].
51 Commonly reported alternative hydrogen donors include primary and secondary
52 alcohols such as methanol, ethanol and isopropyl alcohol (IPA), carboxylic acids
53 including acetic acid (AcOH) and formic acid (FA), and aromatic hydrocarbons (AHs)
54 including tetralin and decalin [4,5]. These hydrogen-rich compounds can supply
55 hydrogen for the HDO reaction through self-decomposition or dehydrogenation [1]. For
56 example, Wang et al. [6,7] reported the deoxygenation of phenol over Ni/Al₂O₃ and Ru
57 based catalysts using methanol and formic acid as hydrogen donor compounds. Guo et
58 al. [8] explored the HDO of p-cresol over a Ru based catalyst with IPA as the hydrogen
59 donor, achieving 98.5% conversion and 84.0% yield of toluene. IPA was also found to
60 be effective in humins conversion [9]. Vasiliadou and Lemonidou reported the HDO of
61 glycerol at 220 – 250 °C. The highest 1,2-propanediol yield of 53% was obtained using
62 ethanol as the source of hydrogen [10]. Pajak et al. [11] investigated the hydrogen
63 transfer from tetralin and decalin to coal derived tars, revealing hydrogen transfer from
64 decalin was two times greater than that of tetralin. Similar conclusions were drawn by
65 other researchers when decalin and tetralin were used for bio-oil upgrading through
66 hydrogen transfer deoxygenation [12,13]. In-situ H₂ gas production can also take place
67 through redox reactions. For example, water-gas shift reaction ($\text{CO} + \text{H}_2\text{O} \rightleftharpoons \text{CO}_2 + \text{H}_2$)
68 may occur within the HDO process to supply hydrogen [14].

69 The mechanism of various hydrogen transfer reactions for HDO have been extensively
70 investigated [15–18]. The adsorption and dissociation of molecule hydrogen over
71 various transition metals were reported by Pozzo et al., indicating Ni was the most
72 effective metal in such a process [19]. Experimental and modelling investigation
73 performed by Grilc and Likozar and other researchers revealed that bi-functional Ni-Mo
74 based catalysts are promising for HDO with molecular H₂ [20,21]. Numerical models

75 have been reported as well [22–24] to describe the mechanism and kinetics of catalytic
76 HDO reactions.

77 DFT based studies regarding decomposition of bio-alcohols have been also intensively
78 reported; the decomposition mechanism of methanol over Co(0001) and Co(111),
79 Pd(111), Pt(111), and Ni(111) facets has been investigated, predicting all the C-H bond
80 and C-O bond would cleave prior to the CO bond in these scenarios [25,26]. Alcalá et
81 al. reported the decomposition mechanism of ethanol, predicting that demethylation
82 reaction would happen much faster than dehydroxylation over Pt(111), and methane
83 and CO were more likely to be produced [27,28]. In addition, detailed mechanisms for
84 ethanol decomposition over various transition metals, propanol decomposition over Ni-
85 Fe and Ni-Cu bimetallic facet, and butanol decomposition over Pd(111) facet have
86 been widely reported [28–31].

87 There are limited reports on the DFT modelled decomposition of AHs (as H donors).
88 Kim et al. elucidated the dehydrogenation mechanism of decalin to tetralin and further
89 to naphthalene on the (111) facet of Pd and Pt respectively, revealing that according to
90 the modelling, Pd would outperform Pt by lowering the energy barrier of tetralin
91 conversion to naphthalene by 0.31 eV [32].

92 Regarding the bio-acids, the decomposition of FA over Cu (111) facet has been
93 analysed by DFT, predicting the most favourable reaction pathway was $\text{HCOOH} \rightarrow$
94 $\text{HCO} \rightarrow \text{CO}$ [33]. The decomposition of acetic acid over a variety of catalysts were also
95 reported [34,35]. Xinbao et al. investigated the decomposition mechanism of AcOH
96 over Co (111) stepped facet, and revealed that the reaction pathway follows CH_3COOH
97 $\rightarrow \text{CH}_3\text{CO} \rightarrow \text{CH}_2\text{CO} \rightarrow \text{CH}_2 \rightarrow \text{CH}$ [36]. Although, there are other different reaction
98 mechanisms for AcOH decomposition proposed in the literature [37–39]. The detailed
99 description of the decomposition of bio-acids over different catalysts, especially over
100 base transition metals, are still unclear and scarce. Moreover, previous studies have

101 reported the performance of various hydrogen donors, however most of them cannot
102 be compared because different catalysts were used. There are very few reports on the
103 evaluation of the reactivity of different hydrogen donor compounds over one selected
104 catalyst and their capacity for HDO reactions.

105 Hence, this research is aimed at the evaluation and systematic comparison between
106 two bio-based acidic hydrogen donors, since they abundantly exist in the primary bio-
107 oil. The decomposition of these carboxylic acids leads to in-situ hydrogen formation,
108 which subsequently can take part in HDO reactions. With respect to catalyst selection,
109 the performance of noble metal based catalysts e.g. Pt and Ru, have been widely
110 studied, while not enough attention have been paid to the base transition metals.
111 Therefore, this study has sought to predict the decomposition of AcOH with a focus on
112 the cleavage of hydrogen related bonds over various transition metals. Ten transition
113 metals (Ni, Mo, Fe, Co, Pt, Rh, Ru, Zn, Cu, and Pd) are compared regarding their
114 binding energy in adsorbing AcOH and the one with strong binding was selected. Then,
115 AcOH and FA are compared with H₂ in terms of their adsorption process and hydrogen
116 donation performance over the most stable facet of the selected catalyst. Electronic
117 density difference (EDD) of the hydrogen donor compounds was analysed to
118 investigate the interface interactions. Bond lengths of the donor compounds were also
119 tracked throughout their decomposition to evaluate the impact of metal catalyst.

120 **2. Computational details**

121 The first-principle density functional theory plus dispersion (DFT-D) calculations were
122 implemented in the Cambridge Sequential Total Energy Package (CASTEP) module
123 available in Materials Studio 2017 R2 from BIOVIA [40,41]. The generalized gradient
124 corrected approximation (GGA) [42] treated by the Perdew–Burke–Ernzerhof (PBE)
125 exchange-correlation potential with long-range dispersion correction via Grimme's

126 scheme was used to calculate the exchange-correlation energy [43]. The On-the-fly
127 generated (OTFG) ultrasoft pseudopotential was employed as the scheme in the
128 representation of reciprocal space for all the elements [44,45]. The plane-wave cut-off
129 energy was set to 500 eV for all the calculations based on its independence test (Fig.
130 S1(a)). The Brillouin zone was sampled using a 2×2×1 Monkhorst-Pack k-point
131 (spacing of 0.04 Å⁻¹) with a smearing of 0.1 eV, based on its independence test (Fig.
132 S1(b)). The self-consistent field (SCF) tolerance was set to 10⁻⁶ eV/atom. All the
133 modelling was performed with a convergence threshold of 10⁻⁵ eV/atom on energy,
134 0.03 eV/Å on maximum force, and 10⁻³ Å on the maximum displacement. No symmetry
135 constraints were used for any modelling. The impact of zero point energy (ZPE) was
136 evaluated for the adsorption of AcOH and FA. It was found that the net ZPE corrections
137 (difference between ZPE of the systems before and after the adsorption) were less
138 than 0.01eV, so that the ZPE correction was not included in the calculations of this
139 study. The computational method is believed to give high precision results, according
140 to the validation of lattice constant for each metal element lattice in this study; the
141 variations between computational and experimental values are less than 0.10 Å for
142 most systems (full comparison is shown in Table S1).

143 The most stable facets of the ten metals were simulated; facet (1 1 1) was simulated
144 for face-centred cubic (FCC) metals including Ni, Cu, Pd, Pt, and Rh, and facet (1 1 0)
145 was simulated for body-centred cubic (BCC) metals of Mo, Fe. For hexagonal close-
146 packed (HCP) metals including Co, Zn, and Ru, facet (0 0 1) was simulated [28,46]. All
147 the metal facet models were created from the optimized metal lattices, and a four-layer
148 slab of P (5×5) super-cell was used with the adsorbate coverage of 1/25ML (Fig. S2).
149 15Å vacuum region was created above the metal facet. The transition state (TS) was
150 completely determined by the LST/QST method, and the TSs for the dominated
151 reaction steps were confirmed by the unique imaginary frequency. Mulliken charges

152 were assigned to each bond to address the bond order [47]. The adsorption energy E_{ad}
153 was determined by Eq.1, where $E_{catalyst}$, $E_{adsorbate}$ and $E_{adsorbate/catalyst}$ are the total
154 energies of clean metal facet, free adsorbate molecule and metal facet with adsorbed
155 molecule respectively. The energy barriers of reactions $E_{barrier}$ were determined by the
156 difference between the transition state and reactant energies, as shown in Eq.2, where
157 $E_{transition\ state}$ and $E_{reactant}$ are the total energies of the transition state and reactant of a
158 reaction.

$$159 \quad E_{ad} = E_{catalyst} + E_{adsorbate} - E_{adsorbate/catalyst} \quad Eq. 1$$

$$160 \quad E_{barrier} = E_{transition\ state} - E_{reactant} \quad Eq. 2$$

161 EDD was determined by Eq.3.

$$162 \quad \Delta\rho = \rho_{adsorbate@Mo(110)} - (\rho_{adsorbate} + \rho_{Mo(110)}) \quad Eq. 3$$

163 where $\rho_{adsorbate@Mo(110)}$ is the electron density of the total adsorbate + Mo(110) system,
164 and $\rho_{adsorbate}$ and $\rho_{Mo(110)}$ are the unperturbed electron densities of the adsorbate and
165 the Mo(110) facet, respectively.

166 Geometry optimization was implemented to every model before energy was calculated.

167 Energy of all the geometries was calculated at 0K in the DFT investigation.

168 **3. Results and discussion**

169 **3.1 Metal catalyst selection based on AcOH adsorption**

170 Most stable facets of ten transition metals were established to identify the metal
171 catalyst that can adsorb AcOH more strongly than the others. The adsorption modelling
172 was carried out by placing AcOH molecule vertically, and binding onto the top site of
173 each metal facet with the carbonyl oxygen atom. More details of the stable adsorption
174 models are shown in the Fig. S2. The adsorption energies are summarized in Table 1,
175 along with relevant geometry parameters (bond length of O-metal, which refers to the

176 distance between the centres of the bounded oxygen atom and the nearest metallic
177 atom, and the corresponding angle of C-O-metal) of the most stable geometry.

178 Table 1. Adsorption energies and geometrical parameters of AcOH on common facets
179 of transition metals

Metal facets	Bond length (Å)	\angle C-O-metal (degree)	Adsorption energy (eV)
Ru (0001)	2.16	143.22	0.91
Mo (110)	2.10	170.16	0.88
Ni (111)	1.93	169.33	0.71
Pd (111)	2.14	141.28	0.70
Fe (110)	1.97	170.92	0.67
Co (0001)	1.95	176.82	0.66
Rh (111)	2.21	175.10	0.60
Pt (111)	2.32	137.75	0.58
Cu (111)	2.15	148.03	0.47
Zn (0001)	2.72	127.95	0.30

180 Note: Considering the effects of adsorption sites and compounds configurations on adsorption energy,
181 more comprehensive adsorption energy of AcOH onto the top three metal facets of Ru, Mo and Ni in
182 different adsorption sites and configurations are calculated and shown in Table 2 and Table. S2.

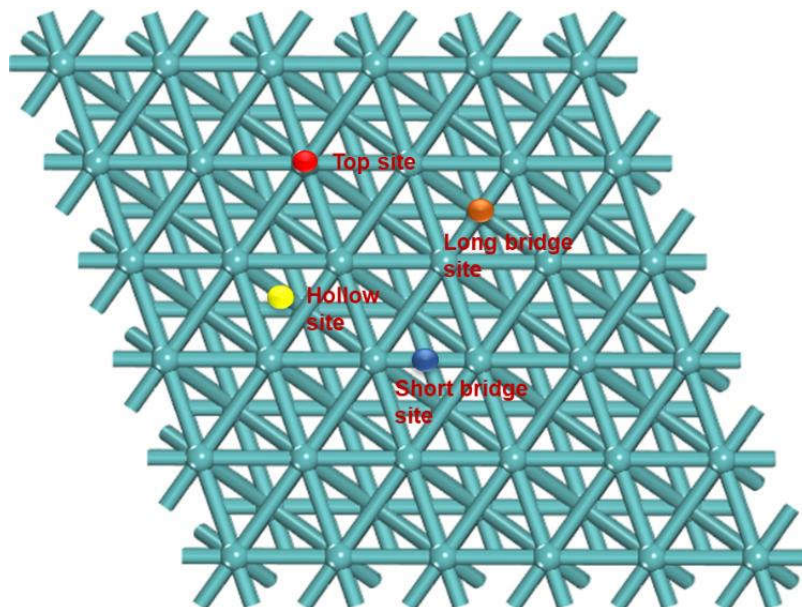
183 The adsorption energy of AcOH onto all of the modelled transition metals facets were
184 less than 1.00 eV. The highest adsorption energy of 0.91 eV and 0.88 eV associated
185 with AcOH adsorption onto Ru (0001) and Mo (110) respectively, followed by 0.71 eV
186 for Ni (111) and 0.70 eV for Pd (111). Adsorption of AcOH on Zn (0001) exhibited the

187 lowest adsorption energy of 0.3 eV. The bonds generated between metal facets and
188 AcOH molecule ranged from 1.93 to 2.72 Å, and the angles generated between C-O
189 bond and O-metal bond ranged between 127.95° and 176.10° for all cases.

190 In the perspective of thermodynamic, the high adsorption energy for Ru, Mo, Ni, Pd
191 implies that chemisorption happens with a strong binding between AcOH molecule and
192 the metals facets. These four metals are commonly known as the catalysts being
193 adopted for the HDO using H₂ gas and for the decomposition of organic compounds
194 with good performance [5,48–50]. Specifically for acids decomposition, Ru, Ni and Pd
195 have been widely reported based on experimental investigation as well as DFT
196 modelling [6,7,34,39,51]. Ru was found quite active in HDO with formic acid as
197 hydrogen donor [7]. Ni was reported to exert high activity in HDO with H₂ gas but poor
198 performance with formic acid as hydrogen donor [6]. Pd is also active but has the
199 potential to lead to the direct formation of CH₄ instead of hydrogen donation [34].
200 Besides, Ru and Pd are noble metals, which would lead to high cost. In comparison,
201 Mo as catalyst has been less investigated thus it is the focus for the further
202 investigations in this study.

203 3.2 AcOH as hydrogen donor on Mo (110) facet

204 The adsorption of AcOH onto Mo (110) facet is investigated in terms of the preferred
205 absorption sites and configuration. Four probable adsorption sites are considered for
206 the adsorption modelling, including top site (Top), short bridge site (SB), long bridge
207 site (LB) and hollow site, as shown in Fig. 1.



208

209

Fig. 1. The probable adsorption sites on the facet of Mo (110)

210

The adsorption of AcOH was simulated over four different adsorption sites, and four

211

configurations for AcOH were compared. The structures of each stable adsorption are

212

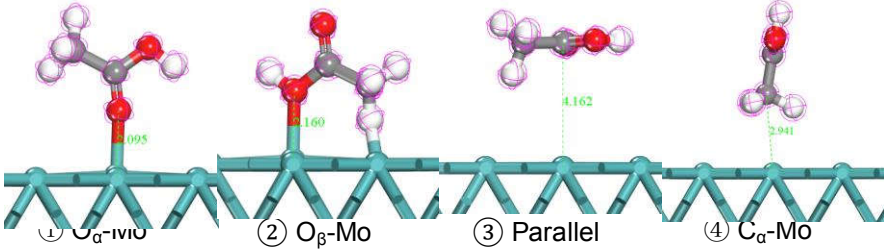
shown in Table 2.

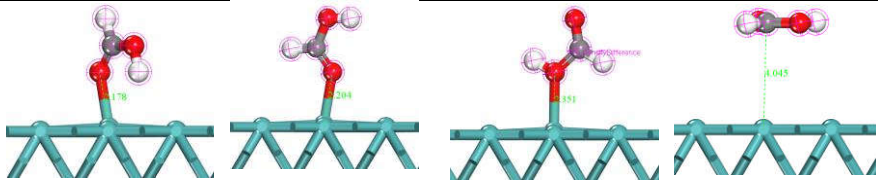
213

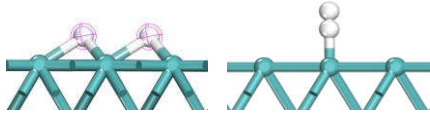
Table 2. Adsorption energy of AcOH, FA and H₂ onto Mo (110) at different sites and

214

configurations

Adsorption Energy of AcOH (eV)				
	① O _α -Mo	② O _β -Mo	③ Parallel	④ C _α -Mo
Top	0.88	0.70	0.28*	0.22*
Short Bridge (SB)	1.24	-	-	-
Long Bridge (LB)	0.28*	-	-	-
Hollow	0.95	-	-	-

Adsorption Energy of FA (eV)				
	① O _α -Mo	② C-Mo**	③ O _β -Mo	④ Parallel
Top	1.15	0.75	0.51	0.18*
Short Bridge (SB)	0.15*	-	-	-
Long Bridge (LB)	0.16*	-	-	-
Hollow	0.12*	-	-	-

Adsorption Energy of H ₂ (eV)		
	① Parallel	② Vertical
Top	0.57	0.56
Hollow	1.64	-

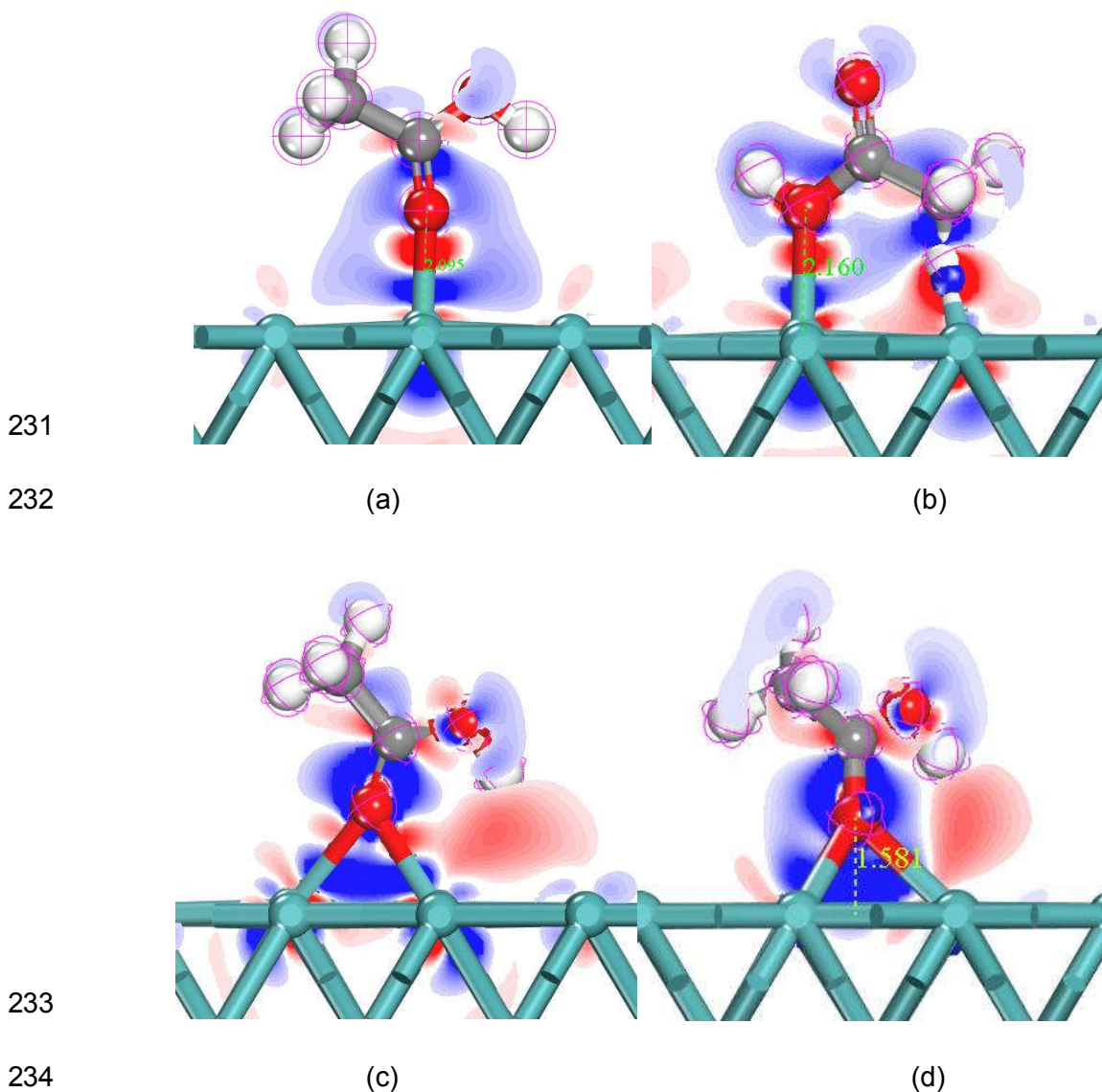
215 * Only stable physical adsorption observed

216 ** Transformed binding from C-Mo to O-Mo (as shown) after geometry optimization

217 Configuration ① led to the highest AcOH adsorption energy of 0.88 eV compared to
 218 other configurations, followed by configuration ④, for 0.70 eV. While configuration ②
 219 and ③ resulted in lower adsorption energies of 0.28 eV and 0.22 eV respectively.
 220 Regarding different adsorption sites based on configuration ①, AcOH was able to
 221 develop strong bindings on to the top, SB and hollow site of Mo facet, resulting in the
 222 adsorption energy of 0.88 eV, 1.24 eV and 0.95 eV respectively. The adsorption of
 223 AcOH onto LB site gave rise to the adsorption energy of 0.28 eV.

224 The results reveal that AcOH molecule most likely will adsorb on the SB site of Mo (110)
 225 facet through the binding between O^α and Mo facet, leading to the highest adsorption
 226 energy. Carbon and hydrogen in the molecule are found hardly to form strong bond
 227 with the Mo facet independently. The adsorption onto the positions of Top ① and SB
 228 ②, and hollow are likely to be chemical adsorption, because of the large adsorption

229 energy. To confirm this, electrons migration between the interfaces was investigated by
230 the calculation of EDD, as shown in Fig. 2.

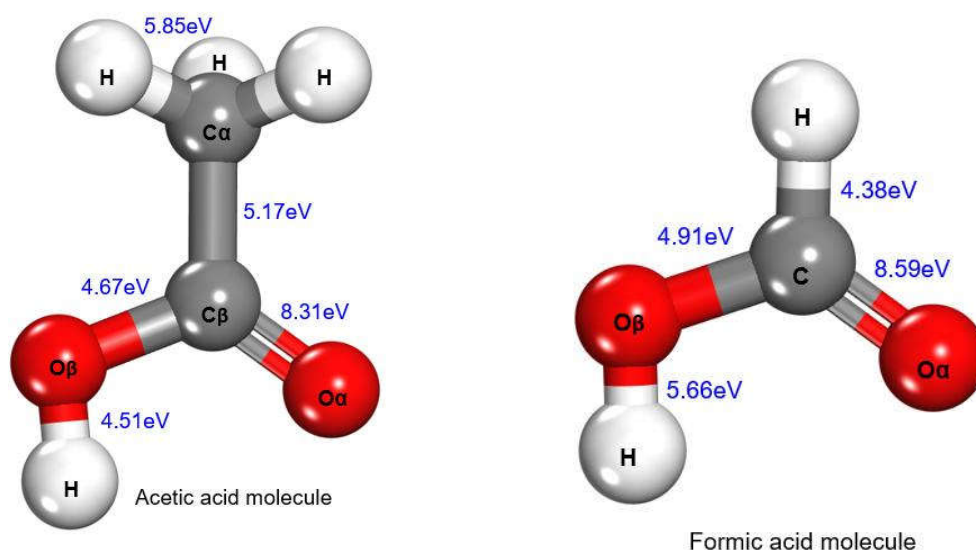


235 Fig. 2. Colour mapping of electron density difference (threshold value: ± 0.05
236 electrons/ \AA^3) for AcOH adsorption configurations of (a) Top ①, (b) Top ②, (c) SB, and
237 (d) hollow. (Loss of electrons is indicated in blue, while electron enrichment is indicated
238 in red)

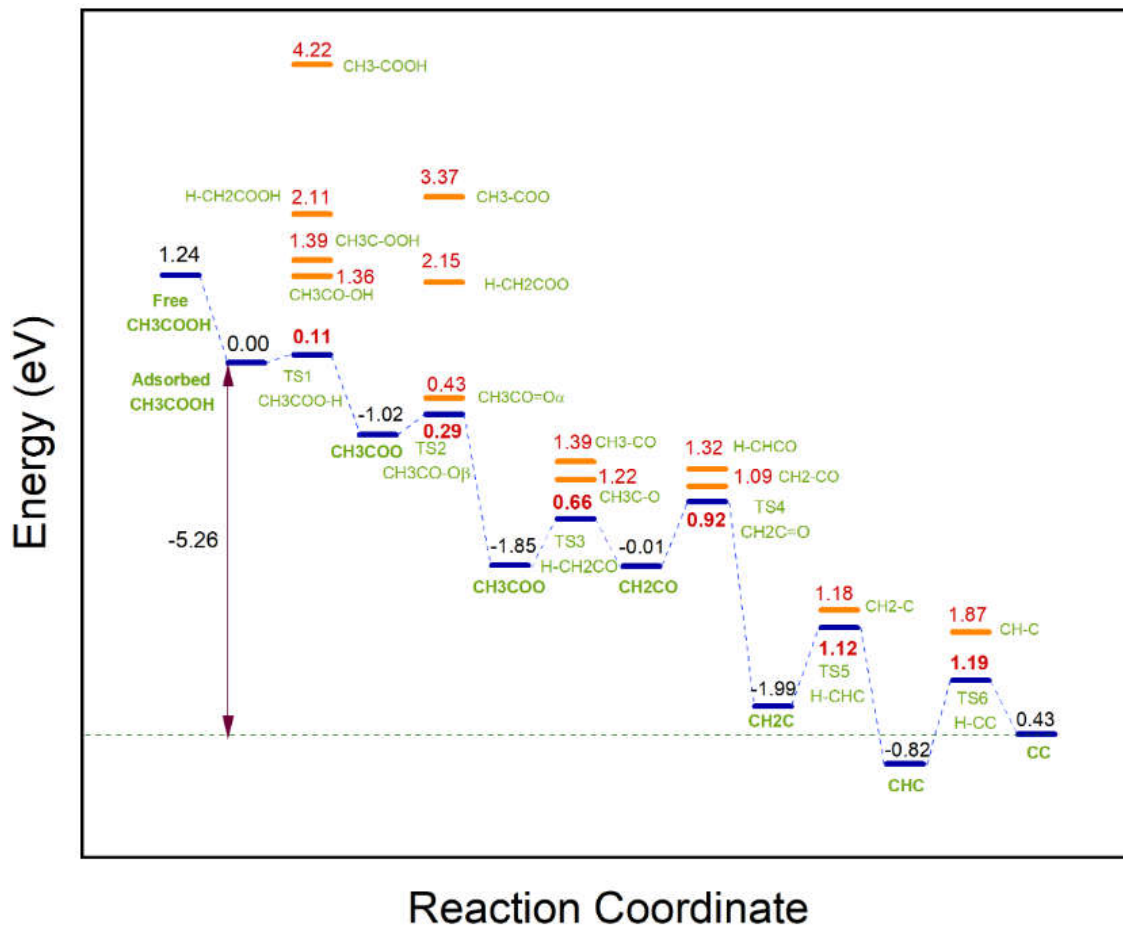
239 Obvious electrons migration around the interfaces of the above four adsorptions
240 indicates that chemical adsorption happened. The adsorption was likely to happen via

241 O^α , where was also the centre for electron migration. When only O^α atom (Fig. 2(a)
 242 and (b)) bonded to the facet, fewer electrons were lost but apparent electrons
 243 enrichment was observed around the O^α atom (Fig. 2(a)) and around the adsorbed
 244 hydrogen atom (Fig. 2(b)). However, severer electron loses happened when AcOH
 245 bound to two Mo atoms through O^α atom over the SB and hollow positions (in Fig. 2(c)
 246 and (d)). These results are in agreement with the highest adsorption energy on these
 247 two sites. They also reveal that the stable adsorption of AcOH on Mo (110) is achieved
 248 by strong electron migration from the molecule to the substrate through the bridge of
 249 $C^\beta - O^\alpha - Mo$.

250 During modelling the decomposition of AcOH over Mo (110), the cleavage energy and
 251 reaction enthalpy were also calculated, in comparison with the free molecular
 252 decomposition of AcOH molecule in the absence of metal catalyst, which is shown in
 253 Fig. 3. The most favourable decomposition pathway of AcOH is illustrated in Fig. 4. The
 254 bond lengths and bond orders for the AcOH molecule and its most probable
 255 intermediates during the decomposition are shown in Table. S3 (a) and (b).



256 Fig. 3. The cleavage energy for the free molecular decomposition of AcOH and FA



257

258

Fig. 4. The decomposition pathways of AcOH over Mo (110) facet

259 For the free molecular decomposition of AcOH, the $C^{\beta}-O^{\alpha}$ bond showed the largest
 260 cleavage energy of 8.46 eV, which was followed by the $C^{\alpha}-H$ bond with 5.85 eV and the
 261 C-C bond with 5.17 eV. The bonds of $O^{\beta}-H$ bond and $C^{\beta}-O^{\beta}$ exhibited similar cleavage
 262 energy of 4.51 eV and 4.67 eV respectively. All the cleavage reactions in free
 263 molecular decomposition were endothermic as there was no new bond formed.

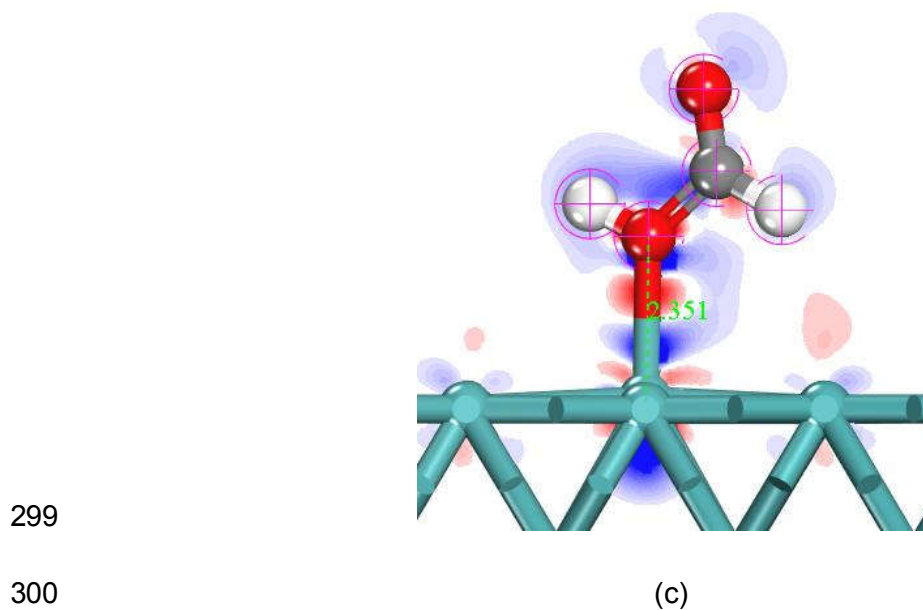
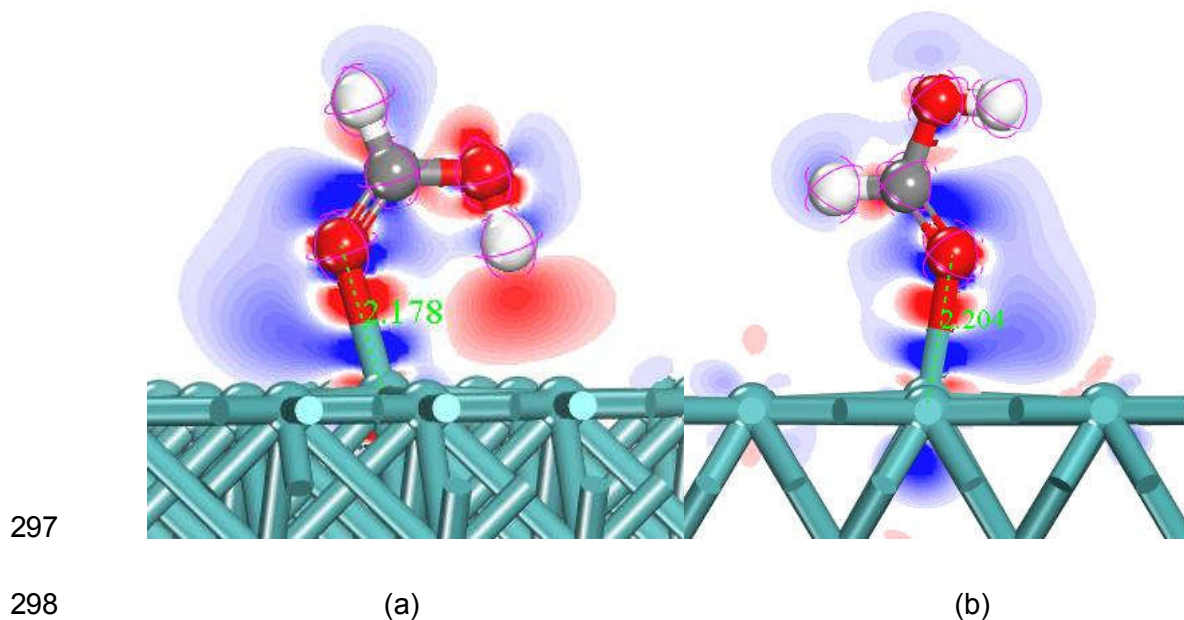
264 The decomposition of AcOH over Mo facet was the most likely to start with the
 265 cleavage of the hydroxyl group with a small energy barrier of 0.11 eV, producing
 266 acetate and one H atom. The acetate could then lose the O^{β} atom and one H
 267 sequentially to form CH_2CO . All the cleavage reactions in the decomposition of AcOH
 268 over Mo facet were exothermic, except for the final H-CC cleavage step, which was
 269 endothermic with $\Delta H = 0.43$ eV.

270 The reaction modelling results reveal that the bulk decomposition of AcOH over Mo
271 (110) is exothermic, which is much more thermodynamically favoured compared to its
272 free molecular decomposition. Besides, the significant decrease in cleavage energy
273 observed during the catalytic decomposition indicates the excellent effect of Mo facet in
274 facilitating the cleavage of AcOH. The most favourable decomposition pathway of
275 AcOH over Mo (110) is $\text{CH}_3\text{COOH} \rightarrow \text{CH}_3\text{COO}+\text{H} \rightarrow \text{CH}_3\text{CO}+\text{O}+\text{H} \rightarrow \text{CH}_2\text{CO}+\text{H}+\text{O}+\text{H}$
276 $\rightarrow \text{CH}_2\text{C}+\text{O}+\text{H}+\text{O}+\text{H} \rightarrow \text{CHC}+\text{H}+\text{O}+\text{H}+\text{O}+\text{H} \rightarrow \text{CC}+2\text{H}+\text{O}+\text{H}+\text{O}+\text{H}$, which is similar to
277 the reported decomposition pathways [36]. The highest energy barrier of 1.19 eV
278 among all the elementary reactions implies that the decomposition of CHC to CC is the
279 rate-determining step. It is also found that the decarboxylation of CH_3COO was
280 suppressed at the beginning, and hydrogen is released during the whole
281 decomposition process. The C-C bond is stable throughout the decomposition, and the
282 remaining C-C anchoring on the Mo facet would result in carbonaceous deposits after
283 further accumulation or they crack to produce CO_2 & CH_4 with hydrogen and oxygen
284 generated in previous steps [34].

285 3.3 FA as hydrogen donor on Mo (110) facet

286 The adsorption energies of FA onto the four different adsorption sites and in four
287 different configurations are specified in Table 2. The configurations with the binding of
288 O^α -Mo (① and ②) showed the highest adsorption energy of 1.15 eV and 0.75 eV
289 respectively. Configuration with O^β -Mo led to the adsorption energy of 0.51 eV. Parallel
290 adsorption (configuration ④) exhibited the lowest adsorption energy of 0.18 eV.
291 Regarding different sites, the adsorption onto the top site led to the highest adsorption
292 energy, followed by SB, LB and hollow sites with adsorption energies of 0.15 eV, 0.16
293 eV and 0.12 eV respectively. These results predict that FA is more likely to adsorb onto
294 the top site of Mo (110) facet through a single O^α -Mo (110) bond. EDD was analysed

295 for the adsorption configurations (①, ②, ③) with high adsorption energies to
296 investigate the interface interaction, as shown in Fig. 5.



301 Fig. 5. Colour mapping of electron density difference (threshold value: +/- 0.05
302 electrons/Å³) for FA adsorption configurations of (a) Top ①, (b) Top ②, and (c) Top ③
303 (Loss of electrons is indicated in blue, while electron enrichment is indicated in red)

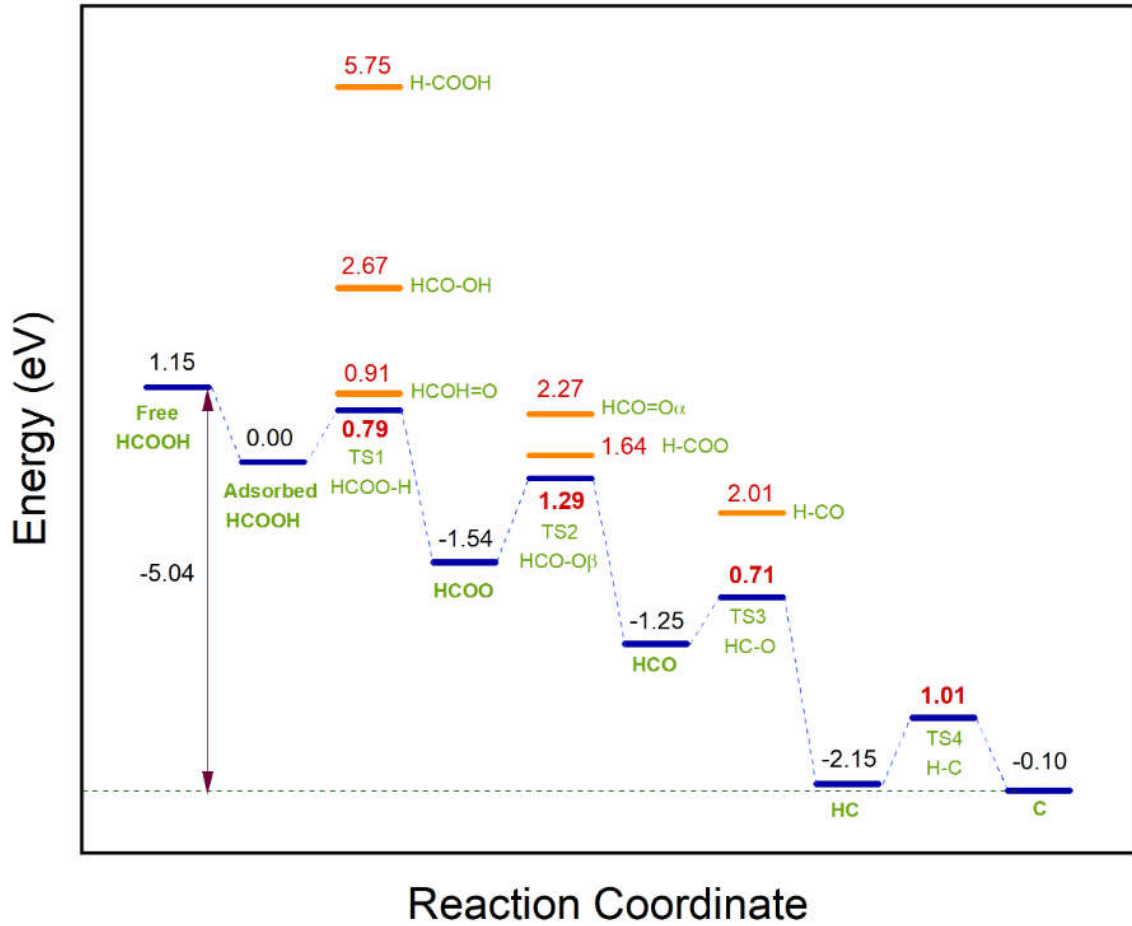
304 The electron migration exhibited in Fig. 5 indicates that all three adsorption
305 configurations are in the form of chemisorbed species, where O atom locates at the
306 centre of electron migration. Significant electrons migration has been observed for the
307 configuration with O^{α} -Mo bond. Fig. 5(a) shows that strong electron lose has taken
308 place around the O^{α} , but apparently electrons were enriched around O^{α} and O^{β} as well
309 as the hydroxyl hydrogen atom. Similar but minor electron migrations were also
310 observed in the other two cases, as demonstrated in Fig. 5 (b) and (c). The strong
311 electron migration implies large adsorption energy, in line with what has been observed
312 in the AcOH adsorption. However, AcOH leads to mainly electron lose, while the
313 binding between FA molecule and Mo (110) facet is found not only results from
314 electron lose, but also from a strong electron enrichment. This could be ascribed to the
315 electron-donating nature of the methyl in AcOH molecule.

316 Based on the reaction modelling for the decomposition of FA, the most probable
317 reaction pathways with the lowest energy barriers are shown in Fig. 6, and the bond
318 lengths and bond orders for the FA molecule and its most probable intermediates
319 during the decomposition are presented in Table S4. (a) and (b). The free molecular
320 decomposition of FA in the absence of metal catalyst is also shown in Fig. 3 for
321 comparison.

322 In the decomposition via the free molecular mechanism, FA showed similar cleavage
323 energy as AcOH for the bond C^{β} - O^{α} (8.59 eV), and slightly lower C-H cleavage energy
324 (4.38 eV) than that of C_{α} -H in AcOH. While the bond C - O^{β} (4.91 eV) and bond O^{β} -H
325 (5.66 eV) were more stable compared to AcOH. All the cleavage reactions in the free
326 molecular decomposition were endothermic as no new bonds were formed.

327 The decomposition of FA over Mo (110) started by the cleavage of O-H with a small
328 energy barrier of 0.79 eV, and was followed by the cleavage of the bonds C - O^{β} and
329 $C=O^{\alpha}$ in sequence with energy barriers of 1.29 eV and 0.71 eV respectively. Finally, the

330 C-H bond cleaved with an energy barrier of 1.01 eV. All the elementary decomposition
 331 reactions were exothermic, as shown in Fig. 6.



332

333

Fig. 6. The decomposition pathways of FA over Mo (110) facet

334

335

336

337

338

339

340

341

342

The modelling results confirm that Mo significantly decreases the cleavage energy of each bond. For instance, the cleavage energy of hydroxyl O-H bond was lowered from 5.66 eV in the free molecular decomposition to 0.79 eV over Mo facet. Besides, the exothermic property of each step in the catalytic decomposition makes it more thermodynamically favoured compared to the free molecular decomposition. The most probable decomposition pathway for FA over Mo facet is $\text{HCOOH} \rightarrow \text{HCOO} + \text{H} \rightarrow \text{HCO} + \text{O} + \text{H} \rightarrow \text{HC} + \text{O} + \text{O} + \text{H} \rightarrow \text{H} + \text{C} + \text{O} + \text{O} + \text{H}$, indicating that O-H and C-H remain the weakest and strongest bond respectively. The highest energy barrier among the elementary reactions was 1.29 eV for the C-O^β cleavage, revealing that it is the rate-

343 determining step. When O^β is cleaved, the bond between C and the other oxygen (O^α)
344 is weakened significantly with the cleavage energy barrier of only 0.71 eV. The
345 cleavage of $C=O^\alpha$ was the exothermic reaction with a significant enthalpy change of
346 2.15 eV. This result indicates that the cleavage of the second C-O bond is the most
347 thermodynamically favoured step for both FA and AcOH. One H atom was released at
348 the beginning of the FA decomposition process and another one at the final step. The
349 single C atom left on the Mo facet might result in carbonaceous deposit or CO_2
350 generation with additional synthesis reactions [33].

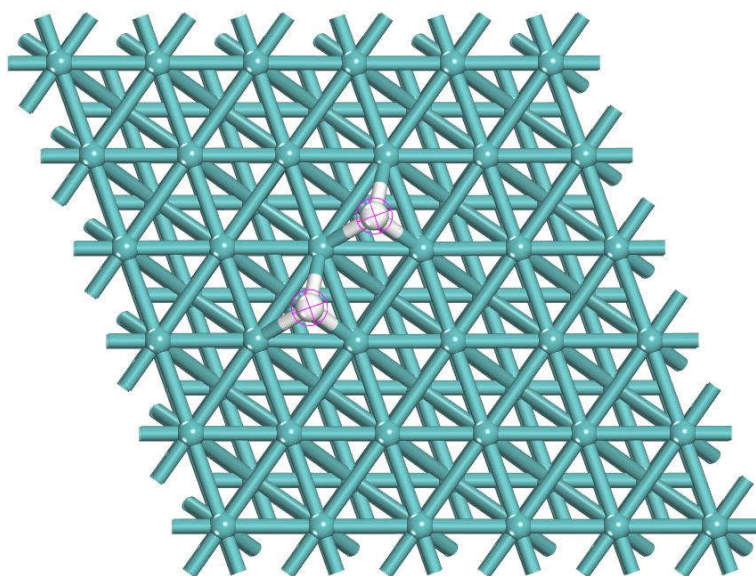
351 The electron migration within the FA molecule under the effect of Mo is not as
352 significant as that of AcOH. However, the loss of electrons in $C=O^\alpha$ still makes it cleave
353 easily prior to C-H bond. The most electron enrichment takes place to the $C-O^\beta$ bond,
354 leading to the highest energy barrier of 1.29 eV for its cleavage reaction.

355 In the catalytic decomposition of AcOH and FA, Mo causes electron migrations
356 between the interfaces. Consequently most of the bonds in the two acid molecules are
357 significantly weakened. For instance, it was found that both decompositions start with
358 hydroxyl O-H cleavage with much cleavage energy compared to the free molecular
359 decomposition. Besides, the $C=O^\alpha$ bonds remain to be the strongest bond in both
360 unadsorbed molecules, but is readily cleaved over Mo facet with much smaller
361 cleavage energy (energy barrier for catalytic reactions), in comparison with the free
362 molecular decomposition. In presence of Mo, AcOH can release two H atoms from
363 hydroxyl and methyl group respectively with low energy barriers, but it requires larger
364 energy to donate another two H atoms from the methylene; the C-H bond becomes
365 stronger when the C was unsaturated inside the molecule. In FA decomposition, the
366 hydroxyl hydrogen is also released at the early stage of its decomposition, however it
367 exhibits higher energy barrier compared to the hydroxyl hydrogen cleavage in AcOH.
368 The other hydrogen in FA is found to be more difficult to release prior to the cleavage

369 of carboxyl oxygen atom, so that it remains to be the final step of the decomposition.
370 The modelling results predict that AcOH possesses a better potential as a hydrogen
371 donor compound over Mo (110) facet.

372 3.4 Dissociation of H₂ over Mo (110)

373 The adsorption of H₂ was modelled and the adsorption energy is presented in Table 2.
374 The results reveal that there were only two possible configurations (vertical and parallel)
375 and two probable sites (top and hollow) for H₂ adsorption. The adsorption showed
376 similar adsorption energy in parallel configuration (0.57 eV) and vertical configuration
377 (0.56 eV). A higher adsorption energy of 1.64 eV resulted from the adsorption onto the
378 hollow position, which is the only plausible adsorption position observed in the
379 modelling other than the top position. It is noteworthy that hydrogen molecule was
380 dissociated into two atoms, anchoring on two hollow positions as shown in Fig. 7,
381 known as dissociative adsorption [52]. The overall dissociative adsorption process of
382 H₂ remained to be exothermic.



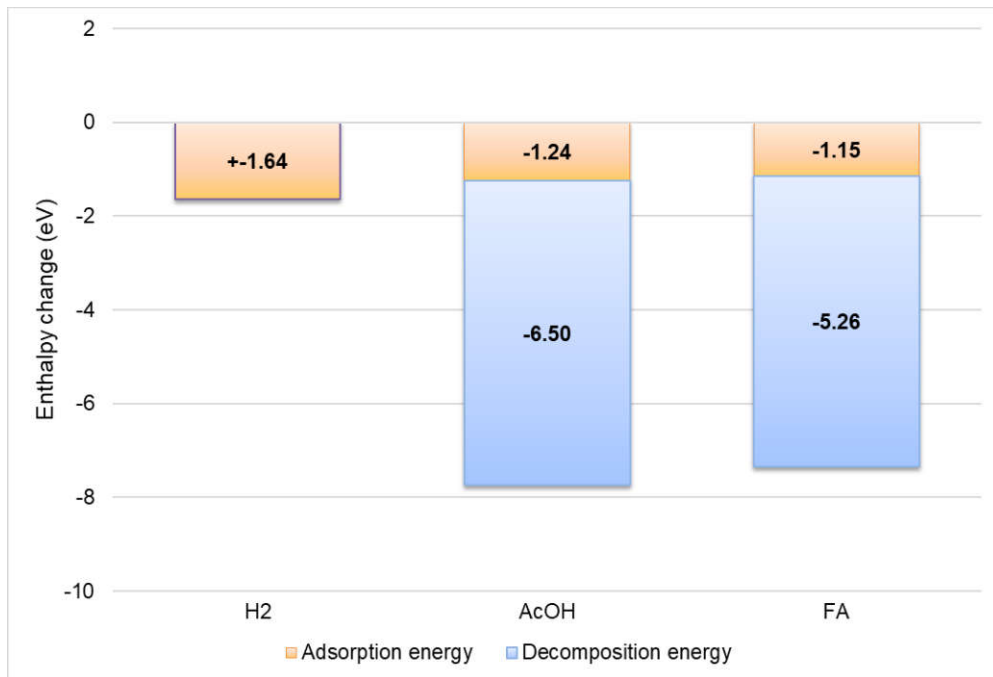
383

384

Fig. 7. Configuration of H₂ adsorption onto hollow position

385 3.5 Comparison of enthalpy changes

386 Modelling results have predicted that the overall decomposition reactions of AcOH and
387 FA over Mo(110) facet are both exothermic, implying the energy released by new
388 binding formation between their intermediates and the Mo facet is more than the
389 enthalpy change for the old binding cleavage [33,36,39]. Thus, the decomposition of
390 both hydrogen donors over Mo (110) facet is hydrodynamically favoured, similar to the
391 dissociative adsorption of H₂. The enthalpy changes for the adsorption and
392 decomposition of AcOH, FA, and H₂ are calculated respectively, and summarized in Fig.
393 8.



394

395 Fig. 8. Overall enthalpy change of adsorption and decomposition of hydrogen donor
396 compounds

397 Hydrogenation and hydrogenolysis reactions normally happen with single hydrogen
398 migration or spillover during the HDO process [53,54], suggesting that the activation of
399 single hydrogen atom would be an essential step for the hydrogen donation. Therefore,
400 the cleavage of metal-single hydrogen bond plays a key role in such a process. The

401 cleavage (activation) enthalpy of the hydrogen-metal bond is calculated and compared
402 with the adsorption and decomposition enthalpy for each hydrogen donor compound,
403 as shown in Fig. 8.

404 Additional calculation for the activation of H atom was performed, and the results show
405 that 3.94 eV was required to activate a single hydrogen atom on Mo (110) facet.
406 Previous results predicts that the enthalpy change for the dissociative adsorption of
407 hydrogen molecule is -1.64 eV, which is bigger than those for AcOH and FA (-1.24 eV
408 and -1.15 eV respectively), nevertheless it is inadequate for one single H atom
409 activation. Due to the exothermic decomposition of AcOH and FA, the overall enthalpy
410 change for the bulk adsorption and decomposition process of AcOH and FA were -6.50
411 eV and -6.19 eV respectively, which are adequate for the activation of H-metal bond.
412 Therefore, the cleavage of H-metal bond could be more facilitated during the
413 decomposition of AcOH and FA. In other words, more hydrogen atoms as well as other
414 decomposed atoms would be likely to migrate and transfer during the decomposition of
415 AcOH and FA compared to the H₂ gas. In this sense, the bio-acids showed good
416 potential to replace H₂ gas as alternative hydrogen donors.

417 **4. Conclusions**

418 The performance of AcOH and FA as hydrogen donors over transition metal facets
419 were investigated and compared with H₂. The adsorption model showed that facets of
420 Ru (0001), Mo (110), Ni (111) and Pd (111) led to the strongest binding to the AcOH
421 molecule among the ten metal facets. Mo (110) was selected as the metal catalyst for
422 further investigating the hydrogen donation of bio-acids as it is a base metal and the
423 lack of atomic-level investigation. EDD analyses revealed that the bindings between
424 bio-acids and Mo were dominated by the electron migration from the molecule to the
425 Mo (110) facet, while electron enrichments in the acid molecule has also been
426 observed for FA adsorption. Mo exhibited positive effect on weakening the bond

427 strength for both acids, and facilitated their cleavage. The reaction model predicted that
428 the most favourable decomposition pathway for acetic acid over Mo (110) was via
429 $\text{CH}_3\text{COOH} \rightarrow \text{CH}_3\text{COO}+\text{H} \rightarrow \text{CH}_3\text{CO}+\text{O}+\text{H} \rightarrow \text{CH}_2\text{CO}+\text{H}+\text{O}+\text{H} \rightarrow \text{CH}_2\text{C}+\text{O}+\text{H}+\text{O}+\text{H}$
430 $\rightarrow \text{CHC}+\text{H}+\text{O}+\text{H}+\text{O}+\text{H} \rightarrow \text{CC}+2\text{H}+\text{O}+\text{H}+\text{O}+\text{H}$, where hydroxyl hydrogen and the
431 methyl hydrogen were more readily to be released than the H atoms from the
432 unsaturated methylene. The most favourable decomposition pathway for FA over Mo
433 (110) facet was through $\text{HCOOH} \rightarrow \text{HCOO}+\text{H} \rightarrow \text{HCO}+\text{O}+\text{H} \rightarrow \text{HC}+\text{O}+\text{O}+\text{H} \rightarrow$
434 $\text{H}+\text{C}+\text{O}+\text{O}+\text{H}$, where the hydroxyl hydrogen can be cleaved and donated at an early
435 stage. Hydrogen showed its undoubtable merits in hydrogen donation because of its
436 dissociative adsorption property over Mo facet. However, compared to the
437 decomposition of H_2 gas, the larger enthalpy change resulted from the exothermic
438 decomposition of the bio-acid compounds would more benefit the activation of
439 decomposed atoms from the catalyst surface, including the hydrogen donation in terms
440 of the single H atom activation and migration. Within the bio-acids, AcOH exhibited a
441 better potential than FA as a hydrogen donor because it released more hydrogen
442 atoms with lower energy barriers. The modelling predicted that AcOH has good
443 potential as an alternative hydrogen donor compound over Mo (110) facet.

444 **Author information**

445 **Corresponding Authors**

446 X.Z.: xiaolei.zhang@strath.ac.uk

447 **Author Contributions**

448 All the authors have given approval to the final version of the manuscript.

449 **Notes**

450 The authors declare no competing financial interest.

451 **Acknowledgement**

452 The authors would like to acknowledge financial support from the Leverhulme Trust
453 Research Grant (RPG-2017-254) and EPSRC First Grant (EP/R010986/1). The
454 authors are also grateful for computational support from the UK Materials and
455 Molecular Modelling Hub, which is partially funded by EPSRC (EP/P020194), for which
456 access was obtained via the UKCP consortium and funded by EPSRC grant ref
457 EP/P022561/1.

458 **References**

- 459 [1] K.M. Isa, T.A.T. Abdullah, U.F.M. Ali, *Renew. Sustain. Energy Rev.* 81 (2018)
460 1259–1268.
- 461 [2] Z. Si, X. Zhang, C. Wang, L. Ma, R. Dong, *Catalysts* 7 (2017) 169.
- 462 [3] Z. Zhang, C. Wang, X. Gou, H. Chen, K. Chen, X. Lu, P. Ouyang, J. Fu, *Appl.*
463 *Catal. A Gen.* 570 (2019) 245–250.
- 464 [4] M.J. Gilkey, B. Xu, *ACS Catal.* 6 (2016) 1420–1436.
- 465 [5] K.W. Cheah, M.J. Taylor, A. Osatiashtiani, S.K. Beaumont, D.J. Nowakowski, S.
466 Yusup, A. V. Bridgwater, G. Kyriakou, *Catal. Today* (2019) 1–11.
- 467 [6] Z. Wang, Y. Zeng, W. Lin, W. Song, *Int. J. Hydrogen Energy* 42 (2017) 21040–
468 21047.
- 469 [7] Y. Zeng, Z. Wang, W. Lin, W. Song, *Chem. Eng. J.* 320 (2017) 55–62.
- 470 [8] T. Guo, Q. Xia, Y. Shao, X. Liu, Y. Wang, *Appl. Catal. A Gen.* 547 (2017) 30–36.
- 471 [9] Y. Wang, S. Agarwal, H.J. Heeres, *ACS Sustain. Chem. Eng.* 5 (2017) 469–480.
- 472 [10] E. Vasiliadou, A. Lemonidou, *Catalysts* 4 (2014) 397–413.
- 473 [11] J. Pajak, V. Krebs, J.F. Marêché, G. Furdin, *Fuel Process. Technol.* 48 (1996)

- 474 73–81.
- 475 [12] D. García-Galindo, M. Gómez-Palmero, M. López-Palmero, E. López, F.
476 Sebastian, in: 24th Eur. Biomass Conf. Exhib. 6-9 June 2016, Amsterdam,
477 Netherlands, 2016, pp. 1727–1733.
- 478 [13] H. Shafaghat, P.S. Rezaei, W.M.A.W. Daud, J. Taiwan Inst. Chem. Eng. 65
479 (2016) 91–100.
- 480 [14] M. Hosseinpour, S. Fatemi, S.J. Ahmadi, M. Morimoto, M. Akizuki, Y. Oshima, E.
481 Fumoto, Appl. Catal. B Environ. 230 (2018) 91–101.
- 482 [15] Q. Song, F. Wang, J. Cai, Y. Wang, J. Zhang, W. Yu, J. Xu, Energy Environ. Sci.
483 6 (2013) 994.
- 484 [16] X. Li, G. Chen, C. Liu, W. Ma, B. Yan, J. Zhang, Renew. Sustain. Energy Rev.
485 71 (2017) 296–308.
- 486 [17] J. Zhang, B. Fidalgo, A. Kolios, D. Shen, S. Gu, Chem. Eng. J. 336 (2018) 211–
487 222.
- 488 [18] D. Ballesteros-Plata, A. Infantes-Molina, E. Rodríguez-Castellón, Appl. Catal. A
489 Gen. 580 (2019) 93–101.
- 490 [19] M. Pozzo, D. Alfè, Int. J. Hydrogen Energy 34 (2009) 1922–1930.
- 491 [20] M. Grilc, B. Likozar, Chem. Eng. J. 330 (2017) 383–397.
- 492 [21] S. Ding, Z. Li, F. Li, Z. Wang, J. Li, T. Zhao, H. Lin, C. Chen, Appl. Catal. A Gen.
493 566 (2018) 146–154.
- 494 [22] B. Hočevar, M. Grilc, M. Huš, B. Likozar, Chem. Eng. J. 359 (2019) 1339–1351.
- 495 [23] J. Zhang, B. Fidalgo, D. Shen, X. Zhang, S. Gu, Mol. Catal. 454 (2018).
- 496 [24] R. Šivec, M. Grilc, M. Huš, B. Likozar, Ind. Eng. Chem. Res. (2019)

497 acs.iecr.9b00898.

498 [25] W. Luo, A. Asthagiri, J. Phys. Chem. C 118 (2014) 15274–15285.

499 [26] Z.C. Kramer, X.K. Gu, D.D.Y. Zhou, W.X. Li, R.T. Skodje, J. Phys. Chem. C 118
500 (2014) 12364–12383.

501 [27] R. ALCALA, J. Catal. 218 (2003) 178–190.

502 [28] P. Ferrin, D. Simonetti, S. Kandoi, E. Kunkes, J.A. Dumesic, J.K. Nørskov, M.
503 Mavrikakis, J. Am. Chem. Soc. 131 (2009) 5809–5815.

504 [29] Y. Choi, P. Liu, Catal. Today 165 (2011) 64–70.

505 [30] M. Myint, Y. Yan, J.G. Chen, J. Phys. Chem. C 118 (2014) 11340–11349.

506 [31] F. Gao, Y. Wang, L. Burkholder, C. Hirschmugl, D.K. Saldin, H.C. Poon, D. Sholl,
507 J. James, W.T. Tysoe, Surf. Sci. 602 (2008) 2264–2270.

508 [32] K. Kim, J. Oh, T.W. Kim, J.H. Park, J.W. Han, Y.-W. Suh, Catal. Sci. Technol. 7
509 (2017) 3728–3735.

510 [33] Z. Jiang, P. Qin, T. Fang, Appl. Surf. Sci. 396 (2017) 857–864.

511 [34] Y. Huang, X. Dong, Y. Yu, M. Zhang, J. Phys. Chem. C 121 (2017) 26733–
512 26741.

513 [35] M.D. Esrafil, P. Nematollahi, R. Nurazar, Synth. Met. 215 (2016) 164–169.

514 [36] X. Li, S. Wang, Y. Zhu, G. Yang, P. Zheng, Int. J. Hydrogen Energy 40 (2015)
515 330–339.

516 [37] K.I. Gursahani, R. Alcalá, R.D. Cortright, J.A. Dumesic, Appl. Catal. A Gen. 222
517 (2001) 369–392.

518 [38] R. Alcala, J.W. Shabaker, G.W. Huber, M.A. Sanchez-Castillo, J.A. Dumesic, J.
519 Phys. Chem. B 109 (2005) 2074–2085.

- 520 [39] C. Hu, S.-W. Ting, K.-Y. Chan, W. Huang, *Int. J. Hydrogen Energy* 37 (2012)
521 15956–15965.
- 522 [40] B. Delley, *J. Chem. Phys.* 92 (1990) 508–517.
- 523 [41] M.D. Segall, P.J.D. Lindan, M.J. Probert, C.J. Pickard, P.J. Hasnip, S.J. Clark,
524 M.C. Payne, *J. Phys. Condens. Matter* 14 (2002) 2717–2744.
- 525 [42] J.P. Perdew, K. Burke, M. Ernzerhof, *Phys. Rev. Lett.* 77 (1996) 3865–3868.
- 526 [43] S. Grimme, *J. Comput. Chem.* 27 (2006) 1787–1799.
- 527 [44] K. Lejaeghere, V. Van Speybroeck, G. Van Oost, S. Cottenier, *Crit. Rev. Solid*
528 *State Mater. Sci.* 39 (2014) 1–24.
- 529 [45] C.J. Pickard, B. Winkler, R.K. Chen, M.C. Payne, M.H. Lee, J.S. Lin, J.A. White,
530 V. Milman, D. Vanderbilt, *Phys. Rev. Lett.* 85 (2000) 5122–5125.
- 531 [46] I.G. Shuttleworth, *Surf. Sci.* 661 (2017) 49–59.
- 532 [47] F.L. Hirshfeld, *Theor. Chim. Acta* 44 (1977) 129–138.
- 533 [48] M. Grilc, B. Likozar, *Chem. Eng. J.* 330 (2017) 383–397.
- 534 [49] J. Zhang, B. Fidalgo, D. Shen, X. Zhang, S. Gu, *Mol. Catal.* 454 (2018) 30–37.
- 535 [50] A. V. Mironenko, D.G. Vlachos, *J. Am. Chem. Soc.* 138 (2016) 8104–8113.
- 536 [51] B. Pekmezci Karaman, N. Cakiryilmaz, H. Arbag, N. Oktar, G. Dogu, T. Dogu, *Int.*
537 *J. Hydrogen Energy* 42 (2017) 26257–26269.
- 538 [52] J. Greeley, M. Mavrikakis, *J. Phys. Chem. B* 109 (2005) 3460–3471.
- 539 [53] S. Xia, Z. Yuan, L. Wang, P. Chen, Z. Hou, *Appl. Catal. A Gen.* 403 (2011) 173–
540 182.
- 541 [54] A.M. Doyle, S.K. Shaikhutdinov, S.D. Jackson, H.-J. Freund, *Angew. Chemie Int.*
542 *Ed.* 42 (2003) 5240–5243.